Journal of Solid State Chemistry 184 (2011) 1373–1380

Contents lists available at ScienceDirect

Journal of Solid State Chemistry

journal homepage: www.elsevier.com/locate/jssc

ZnO-based hollow microspheres with mesoporous shells: Polyoxometalate-assisted fabrication, growth mechanism and photocatalytic properties

Qiuyu Li [a,b], Weilin Chen [a], Mingliang Ju [a], Lin Liu [a], Enbo Wang [a,*]

[a] Key Laboratory of Polyoxometalate Science of Ministry of Education, Department of Chemistry, Northeast Normal University, Ren Min Street No. 5268, Changchun, Jilin 130024, PR China

[b] Department of Bioengineering, Jilin Business and Technology College, Xi An Road No. 4728, Changchun, Jilin 130062, PR China

ARTICLE INFO

Article history:
Received 12 July 2010
Received in revised form
18 March 2011
Accepted 4 April 2011
Available online 14 April 2011

Keywords:
ZnO
Hollow spheres
Polyoxometalate
Photocatalytic properties

ABSTRACT

With the assistance of Keggin-type polyoxometalate, ZnO hollow microspheres with mesoporous shells were synthesized via a simple solvothermal approach without any templates and surfactants. The observations of morphology and structure performed by field emission scanning electronic microscopy and transmission electron microscopy indicated that the shells of the ZnO hollow spheres were built from nanosheets which were composed of nanoparticles. The transformation of structure and composition of samples were investigated by X-ray diffraction, X-ray photoelectron spectrometry and fourier transform infrared absorption spectroscopy. The formation mechanism of the hollow spheres is proposed based on time-dependent experimental results. The ZnO hollow microspheres exhibited a high photocatalytic activity for decolorization of Rhodamine B under ultraviolet irradiation.

1. Introduction

Controlled fabrication of hollow micro- and nanospheres has attracted growing interest due to not only their special properties such as higher specific surface area, lower density and better permeation, but also to their wide range of applications in catalysis, sensors, drug delivery system and chemical storage [1]. Template approaches, based on hard templates (silica, polystyrene and carbon spheres) [2–4] or soft templates (emulsion droplets and supramolecular micelles/vesicles) [5–7], are effective for the fabrication of hollow spheres. However, the subsequent removal of the templates usually suffers from multistep synthetic processes, which will be disadvantageous for large-scale production and applications. Therefore, it is highly desirable to further explore other template-free methods for large-scale controlled preparation of hollow spheres.

Recently, a number of so-called "one-pot" self-assembly methods based on specific mechanisms concerning the Kirkendall effect [8–10], the Ostwald ripening [11–18] and oriented attachment process [19] are becoming available for preparing inorganic hollow spheres. To date, hollow ZnO [8], Ni_2P [9], PbSe and $NiSe_2$ [10] spheres were synthesized through the Kirkendall effect under hydrothermal conditions. Inorganic hollow spheres, such as SnO_2 [11], Co_3O_4 [12], TiO_2 [13], CuO_2 [14], Fe_3O_4 [15], MnO_2 [16], CdS [17] and Sb_2S_3 [18], were prepared through Ostwald ripening processes under hydrothermal or solvothermal conditions.

Zinc oxide is an environmentally friendly semiconductor with a wide band gap of 3.4 eV and a large exciton binding energy of 60 meV at room temperature, which has received great attention owing to its wide range of modern applications [20]. Thanks to the influence of particle morphology on the properties of materials [21], considerable efforts have been devoted to the development of ZnO with various morphologies, especially to the fabrication of ZnO hollow spheres with novel properties for their further applications [22].

On the other hand, polyoxometalates (POMs) are a unique class of molecular metal–oxygen clusters with exciting properties based on their sizes, shapes, charge densities and reversible redox potentials, most of which are anionic structures [23]. Recently, it has also been introduced into the morphology-controlled fabrication of nanostructures and is becoming more and more remarkable in material synthesis field [24–30]. With the assistance of Keggin-type POMs, our group has also reported the POM-assisted growth of carbon nanotube, silicon nanostructures, iron oxide nanorods, hematite hollow spheres, ZnO solid and hollow spheres [31–36].

In the present researches, ZnO hollow microspheres with mesoporous shells were obtained by a "one-pot" solvothermal

* Corresponding author. Fax: +86 431 85098787.
E-mail addresses: wangeb889@nenu.edu.cn, wangenbo@public.cc.jl.cn (E. Wang).

0022-4596/$ - see front matter © 2011 Elsevier Inc. All rights reserved.
doi:10.1016/j.jssc.2011.04.006

process at low temperature in the presence of Keggin-type POM ($H_4SiW_{12}O_{40}$). Series of experiments showed that the POM was vital for the formation of the hollow microspheres. The photocatalytic activity of the ZnO hollow microspheres was evaluated by examining the degradation of Rhodamine B (RhB) under ultraviolet (UV) irradiation. Moreover, a possible growth mechanism of the as-prepared ZnO hollow spheres was proposed.

2. Experimental section

2.1. Materials

$H_4SiW_{12}O_{40}$ was prepared according to the literature [37]. Zinc acetate dehydrate, ethanol and rhodamine B (RhB) were of analytical reagent grade purchased from Beijing Chemicals Co. Ltd. and used as received without further purification.

2.2. Synthesis of ZnO hollow spheres

In a typical procedure, 0.5 g of Zn $(CH_3COO)_2 \cdot 2H_2O$ was added into 15–20 mL of 1.0×10^{-3} mol/L $H_4SiW_{12}O_{40}$ ethanol solution under magnetic stirring. After a few minutes, the mixture was transferred into a 23 mL Teflon-lined stainless autoclave and heated in a forced conventional air oven at 120 °C for 72 h and then cooled to room temperature naturally. The white precipitates were collected by centrifugation, washed with distilled water and ethanol, and then dried at 60 °C for 6 h.

2.3. Measurement of the photocatalytic activity

The photocatalytic activities of the samples were evaluated by degradation of RhB in an aqueous solution under UV irradiation from a 300 W high-pressure mercury lamp. The experimental procedure was as follows: 50 mg of the photocatalyst was poured into 100 mL of RhB aqueous solution (2.5 mg/L) in a reactor at room temperature under air. Before the UV light was turned on, the solution was continuously stirred for 30 min in dark to ensure the establishment of an adsorption–desorption equilibrium. The concentration of RhB during the degradation was monitored by colorimetry using a UV–752 PC UV–vis spectrometer.

2.4. Characterization

The as-prepared samples were characterized by X-ray power diffraction (XRD) using a Rigaku D/max–IIB X-ray diffractometer with Cu $K\alpha$ ($\lambda = 1.5418$ Å) radiation in a 2θ range from 10° to 90° at room temperature. The microstructure of as-prepared samples were observed by transmission electron microscopy (TEM) using a Hitachi-7500 electron microscope at an accelerating voltage of 120 kV and by field emission scanning electron microscopy (FESEM) using a XL30 ESEM FEG electron microscope at an accelerating voltage of 20 kV. UV–vis absorption spectra were recorded using a 752 PC UV–vis spectrophotometer. The Fourier transform infrared (FTIR) absorption spectrum was obtained in the absorbance mode using a Bio-Rad FTS135 spectrophotometer. Nitrogen (N_2) adsorption–desorption isotherms were measured at liquid nitrogen temperature (77 K) using a NOVA l000 analyzer. The sample was degassed for 6 h at 150 °C before the measurements. Surface areas were calculated by the Brunauer–Emmett–Teller (BET) method from the data in the P/P_0 region 0.05–0.35 and pore sizes by the Barrett–Joyner–Halenda (BJH) method at a relative pressure of 0.95 (P/P_0).

3. Results and discussion

3.1. Structure and morphology

ZnO hollow microspheres with mesoporous shells were readily prepared by solvothermal treatment of a mixture of Zn $(CH_3COO)_2 \cdot 2H_2O$, CH_3CH_2OH and POM ($H_4SiW_{12}O_{40}$) at 120 °C for 72 h. Fig. 1a shows XRD pattern of the as-prepared sample. All diffraction peaks can be indexed as hexagonal phase ZnO (space group: $P63mc$; JCPDS card no. 36-1451) with cell parameters of $a = 3.21$ Å and $c = 5.25$ Å. No characteristic peaks of other impurities were detected.

Fig. 1b shows UV spectrum of the as-prepared ZnO hollow microspheres. There are two main peaks. One peak at 366 nm is attributed to Zn–O of the as-prepared ZnO, the other peak at 245 nm is ascribed to the oxygen–tungsten (O–W) charge-transfer transition of the POM component in the sample [23]. The result indicates that the POM assuredly existed in the as-prepared ZnO hollow microspheres.

To further investigate the composition and chemical state of POM existing in the sample, IR and XPS investigation were carried out. Fig. 2 represents the FTIR spectra in the region of 700–1200 cm^{-1} for pure POM (Fig. 2a) and the as-prepared ZnO powder (Fig. 2b). Fig. 3a shows the W–Oc–W asymmetric stretching vibration frequency at 810 cm^{-1}, the W–Ob–W bending vibration at 993 cm^{-1}, the W–Od bending vibration at 898 cm^{-1}, and the Si–O asymmetric stretching vibration at 1089 cm^{-1} for pure POM. Comparing Fig. 2b with Fig. 2a, a shift of the W–Oc–W bending vibration (at 812 cm^{-1}), the W–Ob–W bending vibration (at 863 cm^{-1}), the W–Od bending stretching

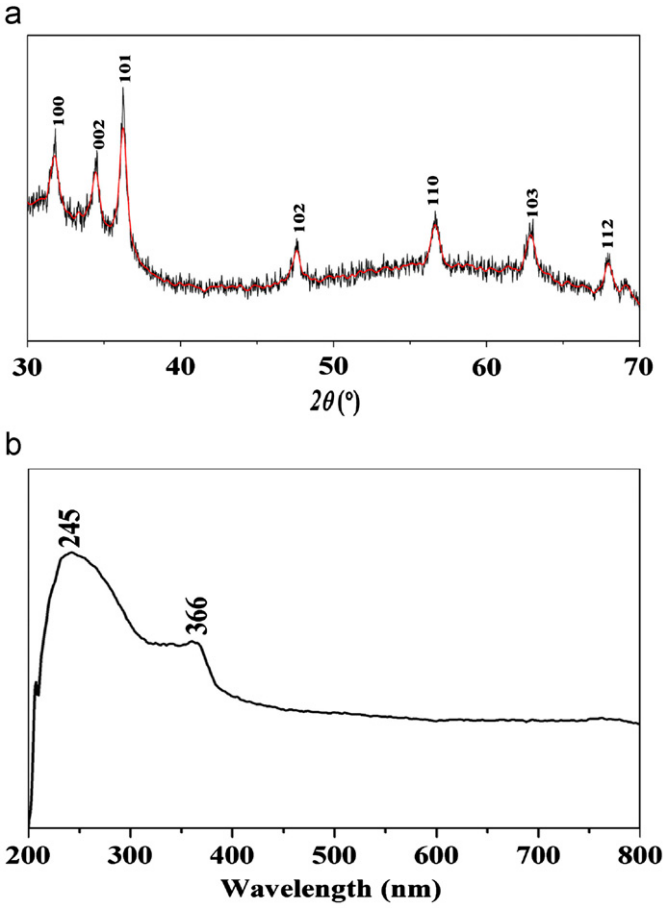

Fig. 1. (a) XRD pattern and (b) UV spectrum of the as-prepared ZnO hollow microspheres.

vibration(at 929 cm^{-1}) and the Si–O asymmetric stretching vibration (at 1026 cm^{-1}), and a decrease of the intensity of the above vibrations were observed [23,36,38]. The differences between Fig. 2a and Fig. 2b imply that there may be an interaction between ZnO and POM anions, confirming the presence of POM in the as-prepared ZnO hollow microspheres. However, no diffraction peaks of the POM can be detected in its XRD pattern (Fig. 1a), which may be probably due to very few POM existing in the as-prepared ZnO powder. XPS spectra of the as-prepared ZnO in Fig. 3a show chemical state of POM. The binding energy located at 39.2 and 35.5 eV is attributed to *W* $4f_{5/2}$ and *W* $4f_{7/2}$ of the POM anions, respectively, suggesting that the POM anions existed in form of the oxidized state [39]. Moreover, O 1s peak of the binding energy located at 530.1 eV (Fig. 3b) is attributed to O^{2-} in the Zn–O bonding on the wurtzite structure. No other peaks of high binding energy (> 530.1 eV) was observed, indicating that there is no chemically absorbed oxygen on the surface of the ZnO [38]. This result implys the POM existed in the as-prepared ZnO through physical absorption instead of chemical bonds. The selected XPS spectrum (Fig. 3c) in the range of 1015–1065 eV displays peaks clearly at 1022.9 and 1046.2 eV, which are assigned to Zn $2p_{3/2}$ and $2p_{1/2}$ of the ZnO, respectively [40].

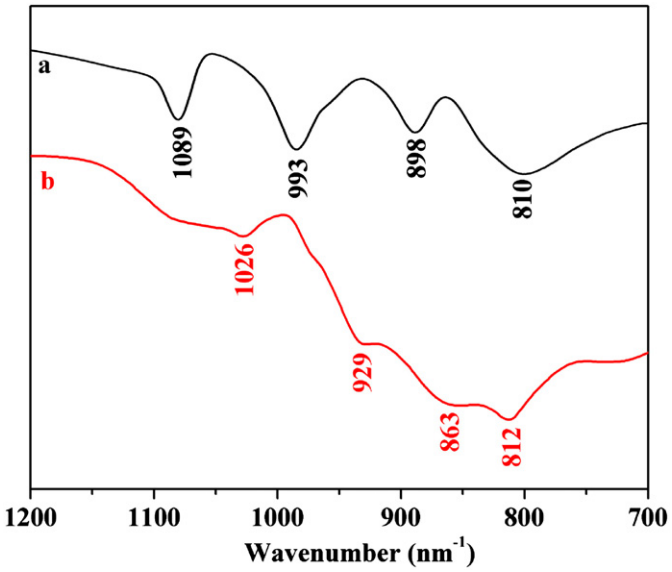

Fig. 2. FTIR spectra of (a) pure POM and (b) the as-prepared ZnO hollow microspheres.

The panoramic morphology of the ZnO prepared with the assistance of POM were studied by SEM. Fig. 4a shows a low-magnification SEM image of the ZnO sample, indicating that the as-prepared ZnO was composed of spherical architectures with a narrow size distribution and diameter of 1.0–1.2 μm. From the high-magnification SEM image (Fig. 4b), the outer surface of the microspheres was rough, which can be seen more clearly from the SEM image (Fig. 4c) of a fragment of the ZnO hollow microspheres. It should be pointed out that the ZnO hollow microspheres are composed of interweaving nanosheets, which grow almost perpendicularly on the spherical surface and make the microspheres look very rugged. Additionally, these nanosheets on the surface make the microspheres have a larger outer surface area than the smooth microspheres, which make this type of microsphere exhibit potential applications such as catalysis or gas sensors. The SEM image (Fig. 4d) of a cracked microsphere indicates that the microsphere have a hollow interior structure and a shell thickness of approximate 80–120 nm. The broken microsphere further demonstrates that the shell consisted of numerous irregular nanosheets.

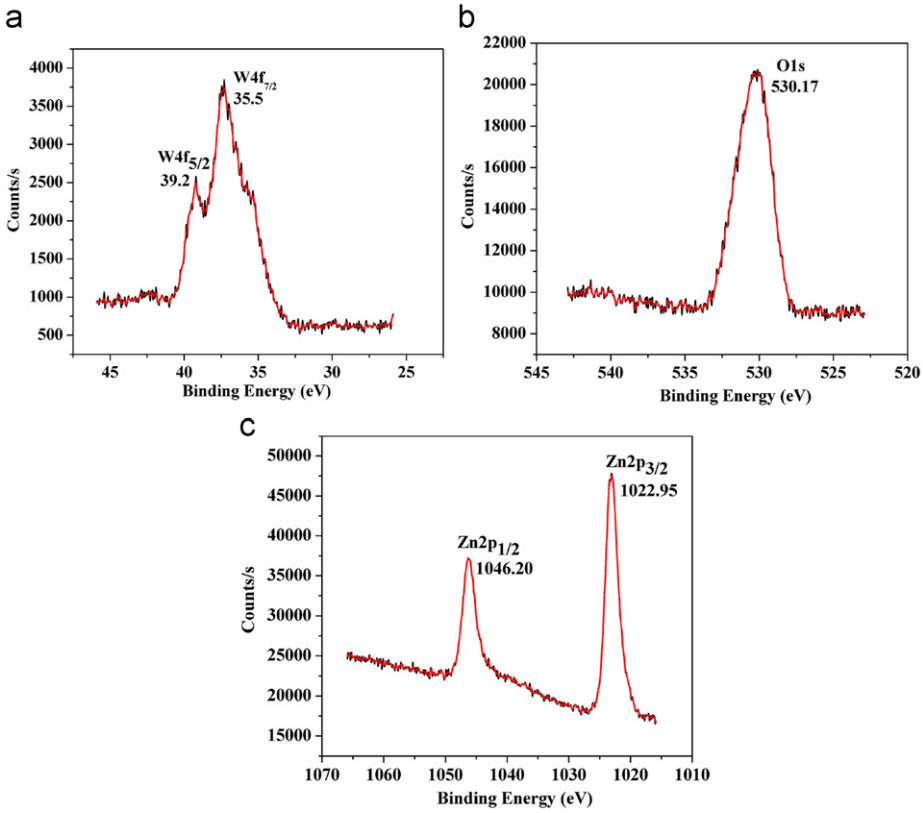

Fig. 3. XPS spectra of the as-prepared ZnO hollow microspheres: (a) W 4*f*, (b) O 1*s*, and (c) Zn 2*p*.

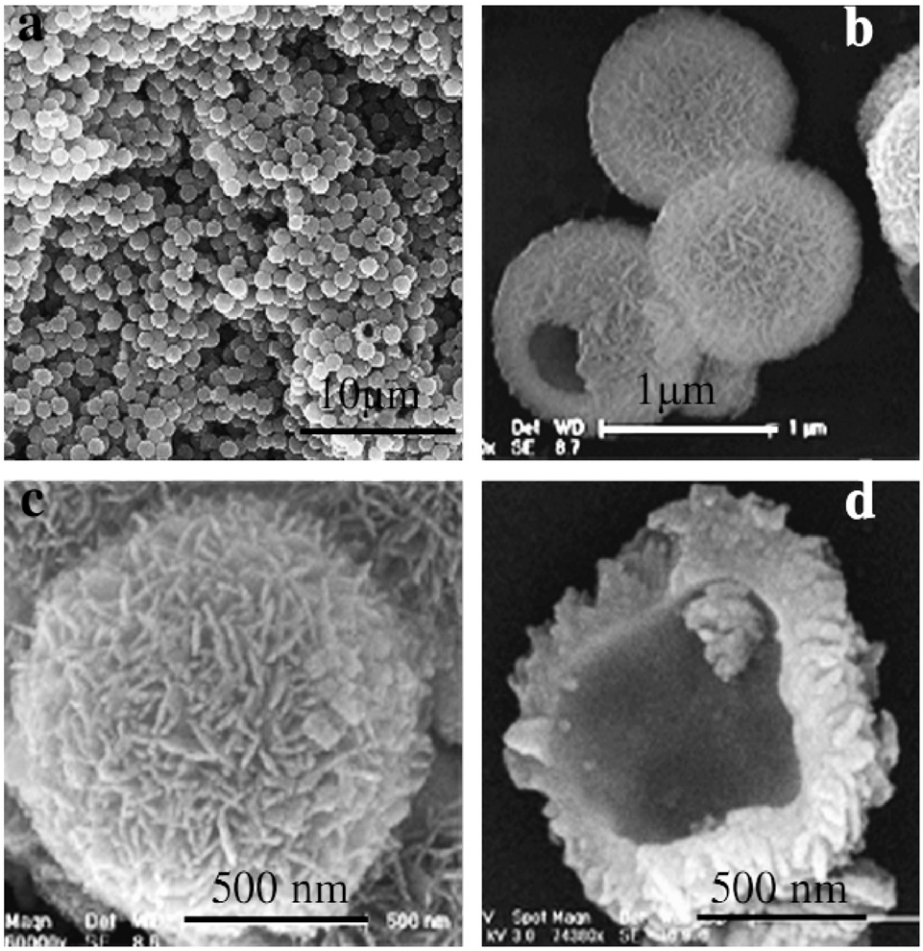

Fig. 4. (a) Low- and (b) high-magnification SEM images of the as-synthesized ZnO hollow microspheres; (c) an intact ZnO microsphere and (d) a broken ZnO microsphere.

To further reveal the morphology and structure of the as-synthesized ZnO hollow microspheres, TEM, SAED and HRTEM analysis were also carried out. Fig. 5a shows a typical TEM image of the as-prepared ZnO sample composed of monodispersed spheres with diameters ranging from 1.0 to 1.2 μm. Moreover, the microspheres possess a hollow interior in the center by an obvious contrast difference between the center portion and the edge of the spherical structures and the shell thickness is about 80–120 nm, in agreement with SEM observations (Fig. 4). Fig. 5b shows TEM image taken near the edge of an individual nanosheet consisting of the ZnO hollow microspheres, clearly revealing that the individual nanosheet is composed of randomly aggregated nanocrystal particles with sizes of about 15 nm. In the nanoparticle subunits, the regular spacing of the observed lattice plane was 0.26 nm, corresponding to the (0 0 2) planes of ZnO hexagonal phase. In addition, detailed observation from the HRTEM images (Fig. 6c) clearly confirms the ZnO nanosheets have many irregular pores with about 2 nm in size, which resulted from the inter-space of nanoparticles assembling nanosheets. However, the pore structures in the ZnO nanosheets are not observed from SEM images (Fig. 4c and d) due to very small poresize.

To further investigate information of the pores in the nanosheet, gas (N_2) absorption measurement was performed. Fig. 6 displays the N_2 adsorption–desorption isotherm of the ZnO hollow microspheres, indicating the existence of pores on the shell of the ZnO hollow spheres. The isotherm has a distinct hysteresis loop observed in the P/P_0 range of 0.45–0.95, which is the characteristic of mesoporous materials. The BET surface area of the ZnO hollow spheres is about 93.10 m^2/g calculated from the data in the P/P_0 region of 0.05–0.45. The inset in Fig. 6 shows the BJH pore-size distribution curve of the ZnO hollow spheres. There are two kinds of pores with a narrow distribution apex centered at 2 and 5 nm, respectively, which are attributed to the inter-nanoparticle space [41], in agreement with the HRTEM observations of the hollow ZnO spheres (Fig. 5c).

3.2. Growth mechanism

In order to understand the growth mechanism of the ZnO hollow microspheres, time-dependent experiments have been carried out and the morphology evolution of the ZnO assemblies over time has also been investigated by TEM. Fig. 7a–d depicts TEM images of the samples obtained with certain reaction time intervals. When the reaction time was 6 h, a small amount of sphere-like particles appeared whereas relatively small nanoparticles coexisted (Fig. 7a). When the reaction time was prolonged to 12 h, perfect solid spheres were observed (Fig. 7b). With the elongation of the time to 48 h, asymmetric core-shell structure was observed (Fig. 7c). When the reaction time was further increased to 60 h, the core was smaller than the one for 48 h (Fig. 7d). With the reaction time, evidently, the core in asymmetric core-shell structure was becoming smaller and smaller. Interestingly, the reaction time for 72 h led to the disappearance of the core in asymmetric core-shell structure and the formation

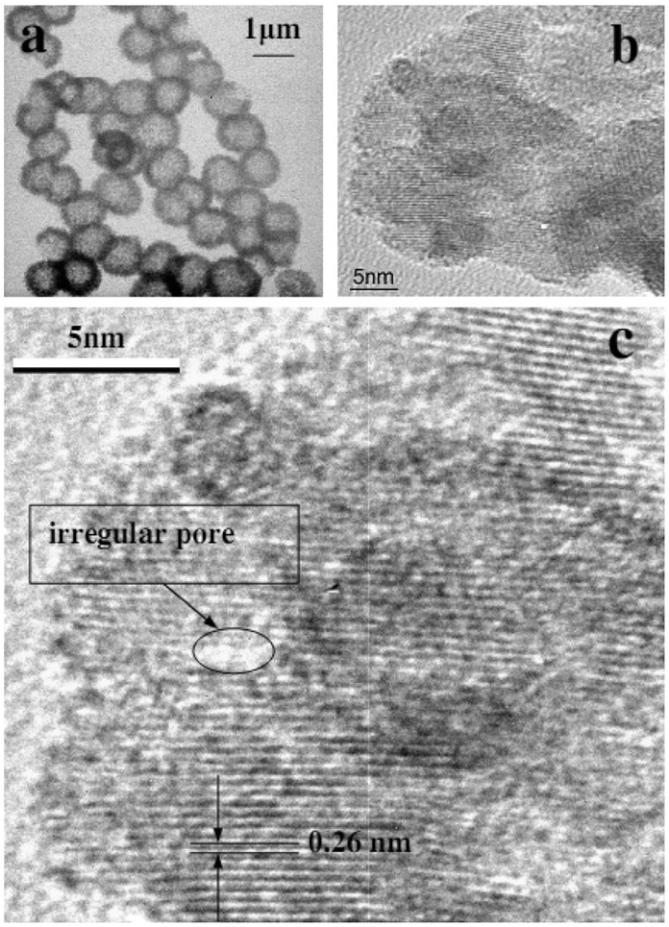

Fig. 5. (a) Typical TEM image of the as-synthesized ZnO hollow microspheres and its corresponding SAED pattern as the inset; (b) TEM image of an individual nanosheet taken from the shell of the microsphere and (c) HRTEM image of a side taken from an individual nanosheet.

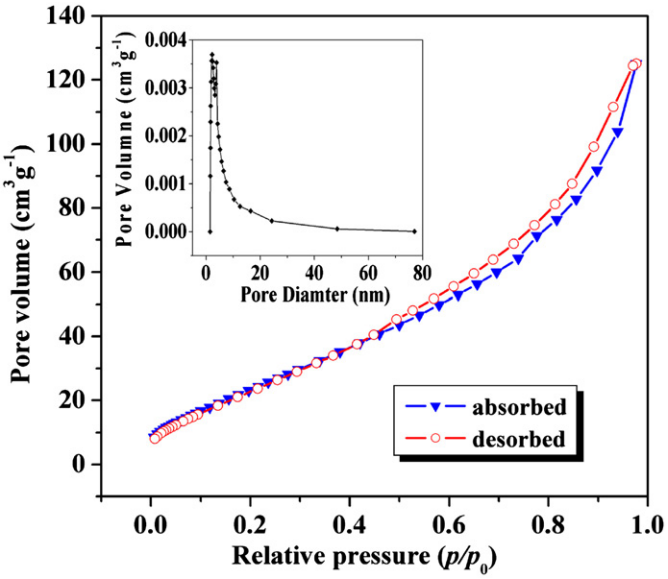

Fig. 6. N_2 adsorption–desorption isotherm of the as-synthesized ZnO hollow spheres and BJH pore-size distribution curve of the as-synthesized ZnO hollow spheres as the inset.

of complete hollow spheres (Fig. 5a). From the time-dependent morphology evolution of the ZnO assemblies, it is believed that the growth of the ZnO hollow spheres may be an oriented aggregation and slow dissolution process.

In order to ascertain effect of POM on the morphology of the ZnO hollow microspheres, compared experiments were performed without POM as shown in Fig. S1 (Supporting Information Available). It was found that hollow microspheres cannot be obtained but only irregular nanoparticles appeared, suggesting that the POM was crucial for the formation of ZnO hollow microspheres.

On the basis of the above experimental results, the whole formation process of the ZnO hollow microspheres can be easily understood which could be divided into three stages as illustrated in Scheme 1. At the first stage, massive small ZnO nanoclusters were momentarily formed due to the catalysis action of the POM for the weak esterification reaction (Scheme 2) of zinc acetate and ethanol [33,42]. On the other hand, hexagonal ZnO crystal has a positively polar zinc face and a negatively polar oxygen face. Thus, negative charge POM was adsorbed at the positive charge zinc face of ZnO through electrostatic action, resulting in temporary stabilization of ZnO nanoclusters [43]. The absorption of POM on the surface of nanomaterials has been reported [30]. At the second stage, the small ZnO nanoclusters preferentially aggregated together and self-assembled to form metastable solid microspheres for the minimization of the total energy of the system. At the final stage, hollow interior structure was formed by dissolution of the nanoclusters in the interior microspheres through a complicated Ostwald ripening process [44,45].

In the current work, both the reaction time and the presence of the POM have been proved to be important controlling factors for the information of the ZnO hollow microspheres. In order to further understand the influences of other factors on the formation process of the ZnO hollow microspheres, more investigations has to be carried out.

3.3. Photocatalytic properties

From the UV spectrum of the as-prepared ZnO hollow microspheres (Fig. 1b), two main peaks exist in UV band. To evaluate the photocatalytic activity of the ZnO hollow microspheres, the degradation of RhB dye as the target dye pollutant in water under UV irradiation was conducted. The characteristic absorption of RhB dye at 550 nm was chosen to monitor the photocatalytic degradation process. Fig. 8 shows the UV–vis absorption spectra of an aqueous solution of RhB (initial concentration: 2.5 mg/L) in the presence of ZnO hollow microspheres (50 mg ZnO in 100 mL aqueous solution of RhB) under UV irradiation. The absorption peaks corresponding to RhB diminished gradually as the exposure time was extended. Significantly, Fig. 9a shows the concentration of RhB barely changed under the UV irradiation without the catalyst, but the suspension containing synthesized catalyst, the color of aqueous RB became pale with the UV irradiation time, suggesting that the degradation of aqueous RB was the result of photoexcited catalysis rather than direct photolysis, which reveals the obvious photocatalytic ability of the ZnO hollow microspheres as shown in Fig. 9b. In addition, it was examined that the ZnO nanoparticles synthesized without the POM degradated aqueous solution of RhB dye under UV irradiation (Fig. 9c). Evidently, photocatalytic ability of the ZnO hollow spheres is superior to that of the ZnO nanoparticles by comparing Fig. 9b with Fig. 9c.

On the basis of the above experimental results, the enhanced photocatalytic activity of the ZnO hollow microspheres compared to ZnO nanoparticles may be attributed to their higher BET specific surface and POM composition. On the one hand, gas (N_2) absorption measurement indicates that the BET surface area of the ZnO hollow spheres is about 93.10 m^2/g (Fig. 6) and that of

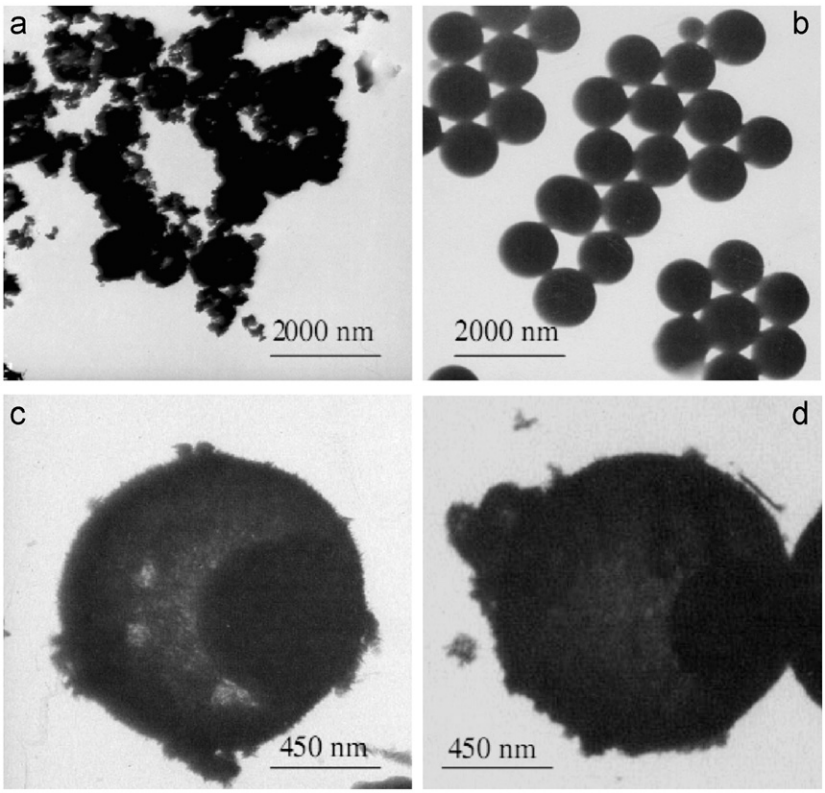

Fig. 7. TEM images of ZnO samples obtained with deferent reaction time: (a) 6 h, (b) 12 h, (c) 48 h and (d) 60 h.

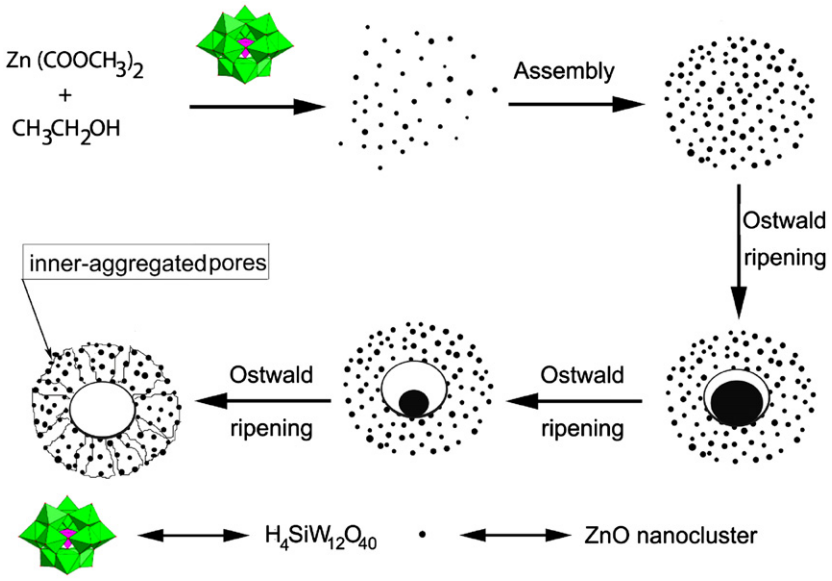

Scheme 1. A proposed formation process of ZnO hollow spheres.

the ZnO nanoparticles is about 18.20 m^2/g (Supporting Information Available). It is well-known that the availability of the surface area is one of the most crucial factors on governing the photocatalytic capabilities. On the other hand, a possible influence of POM existing in the ZnO hollow microspheres on the photocatalytic capabilities was supposed as shown in Scheme 3. When pure ZnO was illuminated by ultraviolet light, the following reactions (Eqs. (1)–(4)) took place on the surface of the photocatalyst [46]. The OH^- and H_2O absorbed on the surface of ZnO will be oxidized into hydroxyl radicals ($\cdot OH$) by photogenerated holes, and then organic dye in the water can be degradated into H_2O and CO_2 by the hydroxyl radicals. Meanwhile, photogenerated electrons and holes can be recombined quickly. Thus, the number of the hydroxyl radicals will be decreased, leading to reduction of the photocatalytic activity. However, ZnO containing POM can probably generate more hydroxyl radicals than pure ZnO under UV illumination as shown in Scheme 3. As we known, POM is a good electron accepter [27] and therefore photoinduced electrons easily transfer from ZnO to POM (Eq. (5)), resulting in separation of photoinduced electrons and holes. On the other hand, the POM^- accepting electron from ZnO will be oxidized into POM and oxyl radicals ($\cdot O_2^-$) (Eq. (6)), whereas the POM^- can react with

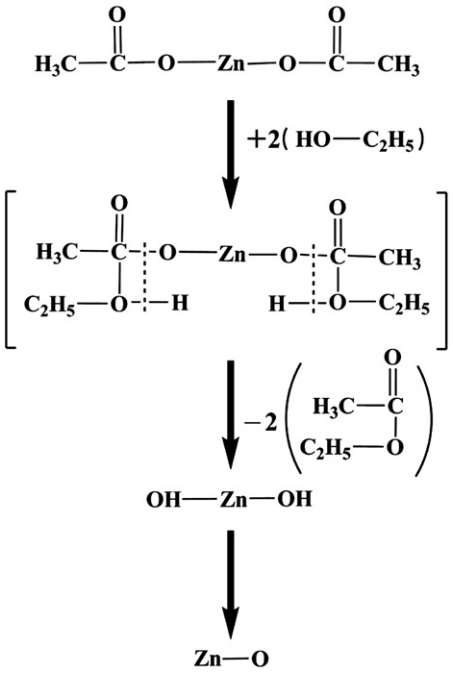

Scheme 2. Reaction formulas for the formation of ZnO crystals.

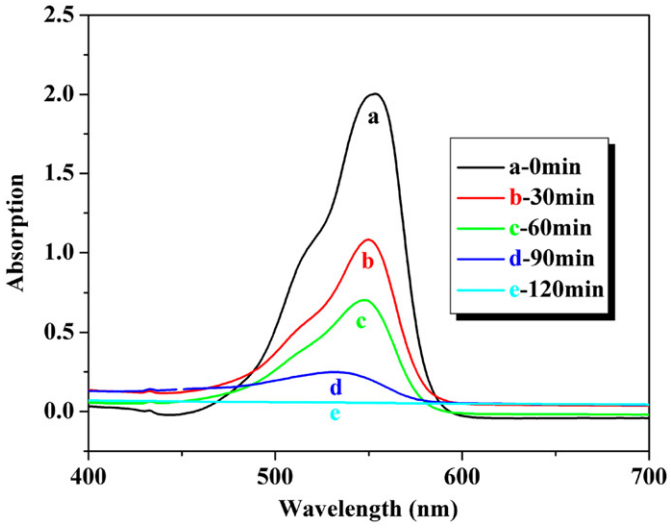

Fig. 8. UV–vis absorption spectra of an aqueous solution of RhB in the presence of the ZnO nanoparticles obtained without POM under UV irradiation.

organic dye into POM (Eq. (7)). Obviously, the POM can effectively prevent from the recombination of photoinduced electrons and holes by its own cycle. In conclusion, the enhanced photocatalytic activity of the ZnO hollow microspheres may be attributed to cooperation effect with POM besides their large surface area.

$$ZnO + h\nu \rightarrow e^{-}\ (CB) + h^{+}\ (VB) \quad (1)$$

$$H_2O + h^{+}\ (VB) \rightarrow \cdot OH + H^{+} \quad (2)$$

$$OH^{-} + h^{+}(VB) \rightarrow \cdot OH \quad (3)$$

$$e^{-}(CB) + h^{+}(VB) \rightarrow \text{energy} \quad (4)$$

$$POM + e^{-}(CB) \rightarrow POM^{-} \quad (5)$$

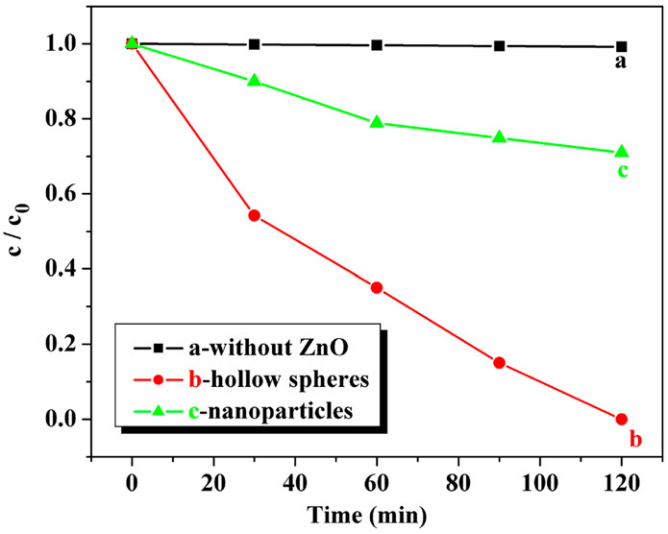

Fig. 9. RhB concentration changes over (a) photolysis, (b) the as-synthesized ZnO hollow spheres and (c) the as-synthesized ZnO nanoparticles.

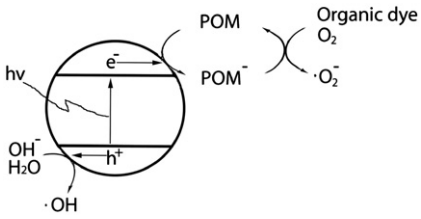

Scheme 3. A proposed photocatalytic process of ZnO containing POM.

$$POM^{-} + O_2 \rightarrow POM + \cdot O_2^{-} \quad (6)$$

$$POM^{-} + \text{Organic dye} \rightarrow POM \quad (7)$$

4. Conclusions

In summary, ZnO hollow microspheres with mesoporous shells were successfully synthesized by one-pot POM-assisted solvothermal treatment at low temperature. The POM was crucial for the formation of the microspheres, which may be expanded to the preparation for other oxides. Additionally, the ZnO hollow microspheres with mesporous shells exhibited a high photocatalytic activity for decolorization of RhB under UV irradiation, which be expected to become potential materials for dealing with the water polluted by dye.

Acknowledgments

This work was supported by the National Science Foundation of China (No. 20371011), the Science and Technology Development Project Foundation of Jilin Province (No. 20060420), the Testing Foundation of Northeast Normal University (No. 201586000/201372000) and the Science Foundation for Young Teachers of Northeast Normal University (No. 20070302/20070312), the Program for Changjiang Scholars and Innovative Research Team in University.

Appendix A. Supplementary materials

Supplementary materials associated with this article can be found in the online version at doi:10.1016/j.jssc.2011.04.006.

References

[1] X.W. Lou (David), L.A. Archer, Z.C. Yang, Adv. Mater. 20 (2008) 1–33.
[2] N.C. Strandwitz, G.D. Stucky, Chem. Mater. 21 (2009) 4577–4582.
[3] M. Yang, J. Ma, C.L. Zhang, Z.Z. Yang, Y.F. Lu, Angew. Chem. Int. Ed. 44 (2005) 6727–6730.
[4] G. Jia, M. Yang, Y.H. Song, H.G. You, H.J. Zhang, Cryst. Growth Des. 9 (2009) 301–307.
[5] Z.G. Teng, Y.D. Han, J. Li, F. Yan, W.S. Yang, Microporous Mesoporous Mater. 127 (2010) 67–72.
[6] A.M. Cao, J.S. Hu, H.P. Liang, L.J. Wan, Angew. Chem. Int. Ed. 44 (2005) 4391–4395.
[7] X. Haolan, W.Z. Wang, Angew. Chem. Int. Ed. 46 (2007) 1489–1492.
[8] B. Liu, H.C. Zeng, J. Am. Chem. Soc. 126 (2004) 16744–16746.
[9] R.K. Chiang, R.T. Chiang, Inorg. Chem. 46 (2007) 369–371.
[10] G.Q. Zhang, W. Wang, Q.X. Yu, X.G. Li, Chem. Mater. 21 (2009) 969–974.
[11] X.M. Yin, C.C. Li, M. Zhang, Q.Y. Hao, S. Liu, L.B. Chen, T.H. Wang, J. Phys. Chem. C 114 (2010) 8084–8088.
[12] C.H. Chen, S.F. Abbas, A. Morey, S. Sithambaram, L.P. Xu, H.F. Garces, W.A. Hines, S.L. Suib, Adv Mater. 20 (2008) 1205–1209.
[13] H.G. Yang, H.C. Zeng, J. Phys. Chem. B 108 (2004) 3492–3495.
[14] J.J. Teo, Y. Chang, H.C. Zeng, Langmuir 22 (2006) 7369–7377.
[15] W. Cheng, K.B. Tang, Y.X. Qi, J. Sheng, Z.G. Liu, J. Mater. Chem. 20 (2010) 1799–1805.
[16] B.X. Li, G.X. Rong, Y. Xie, L.F. Huang, C.Q. Feng, Inorg. Chem. 45 (2006) 6404–6410.
[17] G.F. Lin, J.W. Zheng, R.J. Xu, Phys. Chem. C 112 (2008) 7363–7370.
[18] X.B. Cao, L. Gu, L.J. Zhuge, W.J. Gao, W.C. Wang, S.F. Wu, Adv. Funct. Mater. 16 (2006) 896–902.
[19] H.G. Yang, H.C. Zeng, Angew. Chem. Int. Ed. 43 (2004) 5930–5933.
[20] Z.L. Wang, J. Phys.: Condens. Matter 16 (2004) R829–R858.
[21] X.G. Han, H.Z. He, Q.J. Kuang, Phys. Chem. C 113 (2009) 584–589.
[22] J.G. Yu, X.X. Yu, Environ. Sci. Technol. 42 (2008) 4902.
[23] M.T. Pope, A. Müller, Polyoxometalate Chemistry, Netherlands, 2001.
[24] J. Kim, L. Lee, B.K. Niece, J.X. Wang, A.A.J. Gewirth, Phys. Chem. B 108 (2004) 7927–7933.
[25] P. Garrigue, M.H. Delville, C. Labruge're, E. Cloutet, P.J. Kulesza, J.P. Morand, A. Kuhn, Chem. Mater. 16 (2004) 2984–2986.
[26] P.J. Kulesza, M. Chojak, K. Karnicka, K. Miecznikowski, B. Palys, A. Lewera, A. Wieckowski, Chem. Mater. 16 (2004) 4128–4134.
[27] S. Mandal, D. Rautaray, A. Sanyal, M. Sastry, J. Phys. Chem. C 108 (2004) 7126–7131.
[28] A. Nisar, X.X. Xu, S.L. Shen, S. Hu, X. Wang, Adv. Funct. Mater. 19 (2009) 860–865.
[29] G.J. Zhang, B. Keita, A. Dolbecq, P. Mialane, F. Sécheresse, F. Miserque, L. Nadjo, Chem. Mater. 19 (2007) 5821–5823.
[30] J. Zhang, B. Keita, L. Nadjo, I.M. Mbomekalle, T.B. Liu, Langmuir 24 (2008) 5277–5283.
[31] Z.H. Kang, E.B. Wang, B.D. Mao, Z.M. Su, L. Gao, S.Y. Lian, L. Xu, J. Am. Chem. Soc. 127 (2005) 6534–6535.
[32] Z.H. Kang, C.H.A. Tsang, N.B. Wong, M.L. Zhang, Z.D. Zhang, J.A. Zapien, S.T. Lee, J. Am. Chem. Soc. 129 (2007) 12090–12091.
[33] B.D. Mao, Z.H. Kang, E.B. Wang, C.G. Tian, Z.M. Zhang, C.L. Wang, Y.L. Song, M.Y. Li, J. Solid State Chem. 180 (2007) 489–495.
[34] B.D. Mao, Z.H. Kang, E.B. Wang, C.G. Tian, Z.M. Zhang, C.L. Wang, S.H. Li, Chem. Lett. 36 (2007) 2–3.
[35] Q.Y. Li, Z.H. Kang, B.D. Mao, E.B. Wang, C.L. Wang, C.G. Tian, S.H. Li, Mater. Lett. 62 (2008) 2531–2534.
[36] Q.Y. Li, E.B. Wang, S.H. Li, C.L. Wang, C.G. Tian, G.Y. Sun, J.M. Gu, R. Xu, J. Solid State Chem. 182 (2009) 1149–1155.
[37] J.C. Bailar, Inorganic Synthesis, New York, 1939.
[38] L. Zhang, Y.H. Shen, A.J. Xie, S.K. Li, Y.M. Li, J. Mater. Chem. 19 (2009) 1884–1893.
[39] G.Y. Sun, Y.P. Chang, E.B. Wang, Q.Y. Li, R. Xu, J.M. Gu, E.B. Wang, Dalton Trans. 23 (2009) 4481–4487.
[40] Y. Du, M.S. Zhang, J. Hong, Y. Shen, Q. Chen, Z. Yin, Appl. Phys. A 76 (2003) 171–176.
[41] Q.F. Zhang, T.P. Chou, B. Russo, S.A. Jenekhe, G.Z. Cao, Angew. Chem. Int. Ed. 47 (2008) 2402–2406.
[42] E.B. Wang, Y.B. Tuan, Y.F. Zhang, Y.X. Zhou, Chin. J. Catal. 14 (1993) 147–149.
[43] X. Wang, C.J. Summers, Z.L. Wang, Nano Lett. 4 (2004) 423–426.
[44] B. Liu, H.C. Zeng, Small 1 (2005) 566–571.
[45] Y. Chang, J.J. Teo, H.C. Zeng, Langmuir 21 (2005) 1074–1079.
[46] H.B. Lu, H. Li, L. Liao, Y. Tian, M. Shuai, J.C. Li, M.F. Hu, Q. Fu, B.P. Zhu, Nanotechnology 19 (2008) 045605–04561.